ACS OMEGA

http://pubs.acs.org/journal/acsodf

Article

Intrinsic Magnetic Proximity Effect at the Atomically Sharp Interface of $Co_xFe_{3-x}O_4$/Pt Grown by Molecular Beam Epitaxy

Shoto Nodo,* Ichiro Yamane, Motohiro Suzuki, Jun Okabayashi, Seiya Yokokura, Toshihiro Shimada, and Taro Nagahama

Cite This: *ACS Omega* 2023, 8, 24875−24882

Read Online

ACCESS | Metrics & More | Article Recommendations | Supporting Information

ABSTRACT: $Co_xFe_{3-x}O_4$(CFO)/Pt bilayers prepared by molecular beam epitaxy were investigated for the anomalous Hall effect and X-ray magnetic circular dichroism (XMCD). We found that the anomalous Hall effect originates from a magnetic proximity effect at the CFO/Pt interface. The XMCD signal in the Pt *L*-edge was obtained only for the sample deposited at 600 °C, indicating that the magnetic proximity effect is sensitive to the interface structure. Transmission electron microscopy images of the CFO/Pt interface and XMCD measurements of Co and Fe *L*-edges do not provide direct evidence for interfacial atomic diffusion or alloying. In summary, these results suggest that the magnetic proximity effect is robust for transport properties, such as the anomalous Hall effect, while the induced magnetic moment depends on slight differences in the interfacial structure, such as the presence or absence of interfacial oxygen ions.

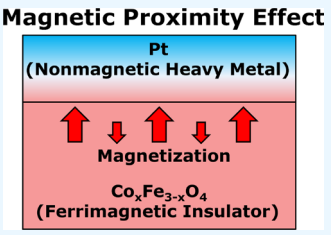

1. INTRODUCTION

Recently, charge-to-spin current conversion phenomena via spin−orbit interactions have been intensively investigated in the field of spintronics. In particular, the spin Hall effect using heavy metal (HM) elements can directly convert a charge current into a spin current,[1,2] and various useful phenomena have been reported in bilayers with ferromagnetic insulators (FMIs) through angular momentum exchange at the HM/FMI interface. Since the spin current can propagate into the FMI but the charge current cannot, the FMI can separate the transport properties between charge and spin currents. The spin Hall magnetoresistance (SMR)[3−5] and spin−orbit torque (SOT) effects[6−8] are examples that have a high potential for application in the operation of high-performance spintronics devices.

In addition to these spin dynamics that occur at the HM/FMI interface, static effects, such as the magnetic proximity effect (MPE),[9] which induces ferromagnetism in a nonmagnetic HM through interfacial exchange interaction, also need to be investigated. The induced ferromagnetism has been examined in terms of the anomalous Hall effect and an anisotropic magnetoresistance effect in the HM layer.[10−13] One significant issue with the MPE is the difficulty of experimentally detecting induced magnetic moments of HMs. First-principles calculations predict that magnetic moments on the order of 10^{-2} μ_B/atom are induced in Pt.[12,14] On the other hand, both X-ray magnetic circular dichroism (XMCD) and X-ray resonant magnetic reflectivity (XRMR) are powerful tools for investigating this induced magnetism. Significant Pt magnetic moment signals cannot be detected by XMCD in the $Y_3Fe_5O_{12}$/Pt[15] and $CoFe_2O_4$/Pt[16−18] systems or by XRMR in the $NiFe_2O_4$/Pt system.[19] Previous XMCD reports of $CoFe_2O_4$/Pt grown by pulsed laser deposition (PLD) found alloying at the interface in Pt deposited at high temperatures (400 °C).[20] Since this magnetic signal originates not from the MPE but from the alloying at the interface, the appearance of induced magnetic moments in Pt largely depends on the interfacial structures. This suggests that the MPE depends on the growth temperature and growth mode, such as molecular beam epitaxy (MBE), PLD, or sputtering deposition. This arises from the difference in kinetic energies, with atoms deposited by MBE having lower kinetic energies than those deposited by sputtering, which suppresses the diffusion of atoms at the interfaces. In the first-principles calculation, even with alloying, slight differences in the interface structure such as differences in the Pt neighbor atom greatly contribute to the magnetic moment of Pt.[12,14] Therefore, it is necessary to investigate the interface structure in more detail in order to understand the MPE in HM/FMI.

In this study, we employ MBE for the growth of CFO/Pt bilayers to understand the MPE by comparison with an interface prepared by sputtering in a previous study.[20] The interface structure of CFO/Pt can also be controlled by the deposition temperature of Pt. Therefore, we aim to clarify the interfacial atomic structures and element-specific electronic and magnetic structures in CFO/Pt by high-resolution scanning transmission electron microscopy (HR-STEM) and

Received: February 12, 2023
Accepted: June 15, 2023
Published: July 4, 2023

https://doi.org/10.1021/acsomega.3c00935
ACS Omega 2023, 8, 24875−24882

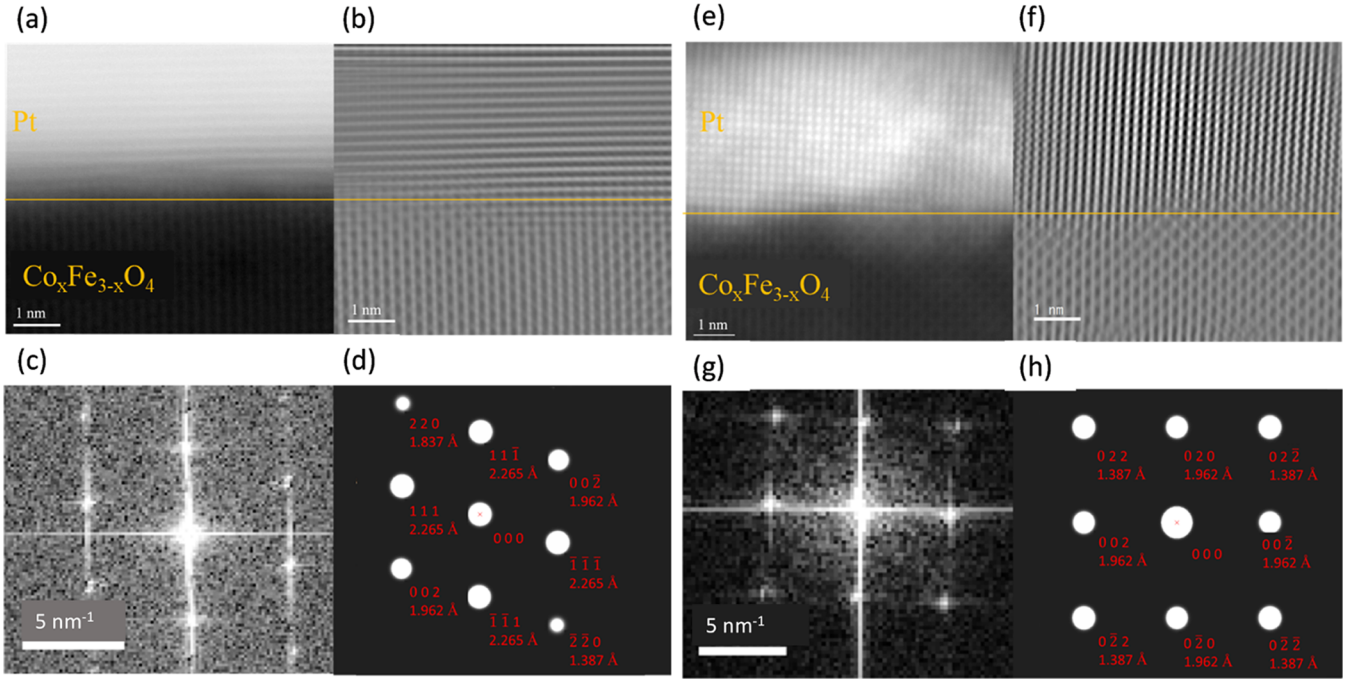

Figure 1. (a–d) HR-STEM images and analysis of CFO/Pt@100. (a) HAADF image of the $Co_xFe_{3-x}O_4$/Pt interface. (b) FFT filtering image of the $Co_xFe_{3-x}O_4$/Pt interface. (c) FFT-processed pattern of the Pt layer. (d) Simulated electron diffraction pattern of Pt. The electron beam was introduced along the [1$\bar{1}$0] direction. (e–h) HR-STEM images and analysis of CFO/Pt@600. (e) HAADF image of the CFO/Pt interface. (f) FFT filtering image of the CFO/Pt interface. (g) FFT processed pattern of the Pt layer. (h) Simulated electron diffraction pattern of Pt. The electron beam was introduced along the [100] direction. Panels (d, h) were prepared using ReciPro software.[21]

XMCD depending on the growth conditions by using MBE. Hall measurement in CFO/Pt was also performed to evaluate the MPE.

2. EXPERIMENTAL METHOD

All samples were prepared by reactive MBE at base pressures on the order of 10^{-8} Pa. Sample structures were MgO (001) substrate/ MgO (20 nm)/NiO (5 nm)/$Co_xFe_{3-x}O_4$ (CFO) (50 nm)/Pt (t_{Pt} nm). MgO substrates (20 × 20 × 0.5 mm^3) were ultrasonically cleaned using acetone, ethanol, and water before loading into the MBE chamber. Substrates were annealed at 600 °C for 30 min to remove hydroxide from the surface and to obtain a flat surface. An MgO buffer layer (20 nm) was deposited at 400 °C at a deposition rate of 0.3 Å/s to improve the surface flatness. A buffer NiO layer was deposited at 300 °C at a deposition rate of 0.15 Å/s to prevent Mg atomic diffusion into the CFO layer. The CFO film (50 nm) was fabricated by codeposition of Co and Fe in an atmosphere of oxygen radicals (P_{O^*} = 1.0 × 10^{-3} Pa). The CFO growth temperature was set to 300 °C with a deposition rate of 0.3 Å/s, and then, the films were annealed at 450 °C for 30 min in an oxygen atmosphere of 1.0 × 10^{-3} Pa. To improve the perpendicular magnetic anisotropy of CFO, an Fe-rich composition was employed, typically Co/Fe = 1:10. Perpendicular magnetic anisotropy is considered advantageous for observing anomalous Hall effects in Hall measurements, where a magnetic field is applied perpendicular to the plane. Subsequently, the Pt layer was deposited at a deposition rate of 0.2 Å/s. Several films were prepared with Pt layers deposited at various temperatures (100, 200, 300, 400, 500, and 600 °C).

In order to evaluate the MPE systematically, the thickness of the Pt layer was fixed at 1 nm to enhance the MPE and maintain the metallic conductance, except for the transmission electron microscopy observation and the evaluation of thickness dependence of Pt.

For the Hall effect measurements, the CFO/Pt film was patterned into Hall bars (length, l = 1500 μm; width, w = 100 μm) using a standard photolithography system by Ar-ion milling. Direct current (DC) (I = 1 mA) was applied for all Hall measurements, and the transverse voltage was measured by sweeping the magnetic field perpendicular to the plane.

The interfacial structure of CFO/Pt was confirmed by cross-sectional HR-STEM (FEI, Titan3 G2 60–300). Magnetic properties of the $Co_xFe_{3-x}O_4$ films were evaluated by using a superconductive quantum interference device (SQUID) magnetometer (Quantum Design, MPMS3).

X-ray absorption spectroscopy (XAS) and XMCD measurements for the Pt L-edge (2p → 5d transition) were performed at BL39XU in the SPring-8 synchrotron radiation facility. In these measurements, fluorescence yield mode was employed. The photon helicity was fixed and a magnetic field of ±1.9 T was applied parallel to the incident polarized hard X-ray beam. For Co and Fe L-edges, XAS and XMCD were performed at BL-7A in the Photon Factory at the High-Energy Accelerator Research Organization (KEK-PF). The photon helicity was fixed, and a magnetic field of ±1.2 T was applied parallel to the incident polarized soft X-ray beam to obtain the absorption signals, defined as μ^+ and μ^- spectra. Total election yield (TEY) mode was adopted, and all measurements were performed at room temperature (RT). The XAS and XMCD measurement geometries were set to normal incidence so that the directions of the photon helicity axis and the magnetic field were parallel and normal to the surface, enabling measurement of the absorption processes involving the normal components of the spin and orbital magnetic moments.

https://doi.org/10.1021/acsomega.3c00935
ACS Omega 2023, 8, 24875–24882

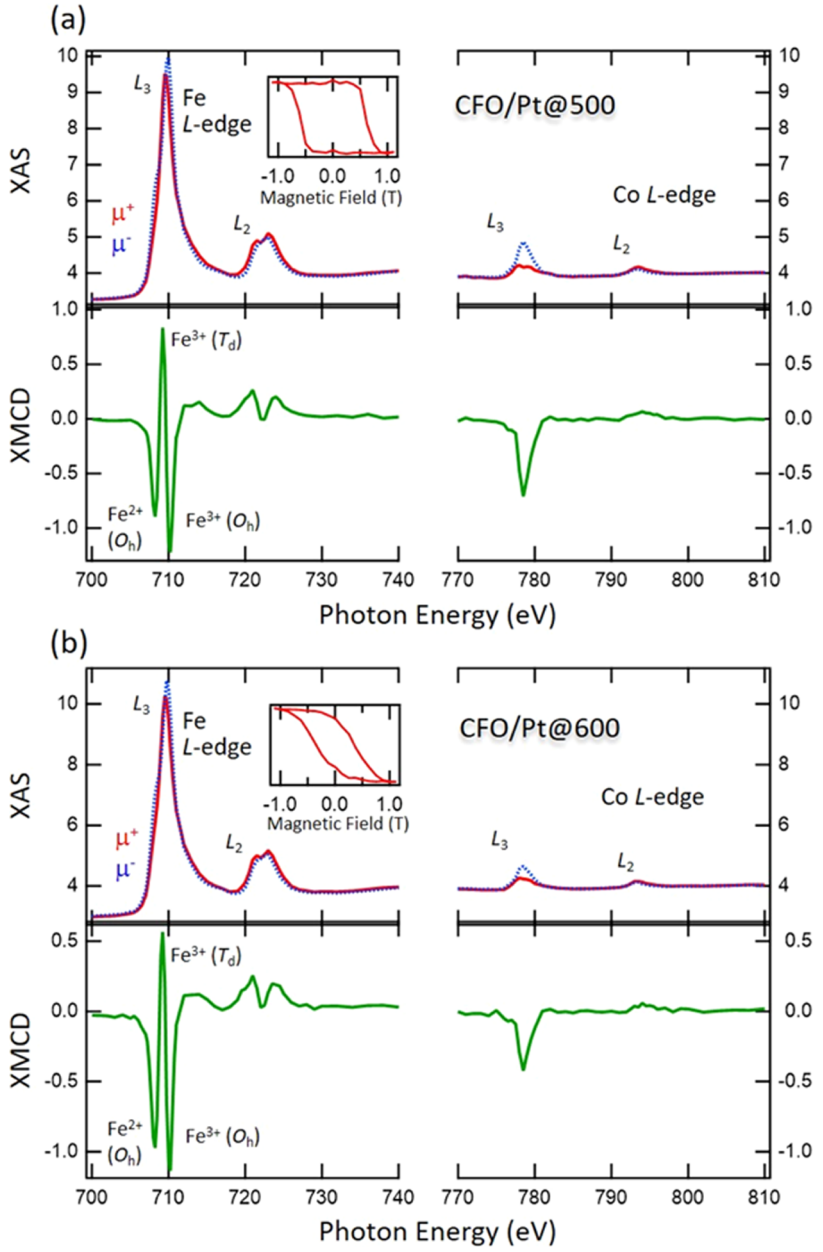

Figure 2. XAS and XMCD spectra of Fe and Co *L*-edges for (a) CFO/Pt@500 and (b) CFO/Pt@600. Insets show the XMCD hysteresis curves taken at the photon energy of $Fe^{3+}(O_h)$.

3. RESULTS AND DISCUSSION

3.1. Interface Investigations. Cross-sectional STEM observations were performed to evaluate the interfacial structure of CFO/Pt. Figure 1a shows the interfacial structure of CFO/Pt in which the Pt layer was deposited at 100 °C (hereafter referred to as CFO/Pt@100). The HR-STEM high-angle annular dark field (HAADF) image and Fourier transformation (FFT) filtering image of Figure 1a exhibited a sharp interface of CFO/Pt@100, indicating negligible atomic interdiffusion at the interface (Figure 1b). The large difference in the contrast between Pt and CFO in CFO/Pt@100 is considered to be attributed to not only the difference in electron scattering capacities but also the technical issue of preparation of the TEM sample such as thicker thickness of the TEM sample at the observation position. An HR-STEM image of the sample of Pt deposited at 600 °C (hereinafter referred to as CFO/Pt@600) is shown in Figure 1e. The slight blurring of the interface was not due to the diffusion of atoms at the interface, but rather due to the blurred contrast between Pt and Co and Fe because of the significantly different electron scattering capacities due to the difference in atomic number. This blurring can be removed by FFT filtering, allowing only the lattice image to be extracted. Figure 1f shows the FFT-filtered image of the CFO/Pt interface of CFO/Pt@600. At the CFO/Pt interface, a discontinuous change from a spinel structure to a face-centered cubic lattice was observed, with negligible Pt diffusion or alloying. This result is different from previous reports of alloy forming at the CFO/Pt interface by Pt deposition at high temperatures (400 °C)[20] because of the difference in the deposition methods. In sputter deposition, diffusion and reaction at the interface are promoted at a deposition temperature of 400 °C since the target atoms possess high kinetic energy at the surface. In MBE, in which

https://doi.org/10.1021/acsomega.3c00935
ACS Omega 2023, 8, 24875−24882

the energy of ad-atoms is low, the diffusion and reaction at the interface during deposition are suppressed, resulting in a relatively sharp interface even at a high temperature of 600 °C. Figure 1c shows an image of the FFT process applied to the Pt layer of CFO/Pt@100, which represents a pseudo-electron diffraction pattern of Pt. This FFT pattern is similar to the electron diffraction pattern of Pt along the $[1\bar{1}0]$ incidence beam, which is one of the crystal band axes of the (111) plane (Figure 1d). This means that Pt was grown nonepitaxially on the CFO (001) plane, thus forming a texture of the Pt (111) plane. This result suggests the growth of the Pt layer along the (111) direction on the CFO (001) plane.[22] However, the FFT-processed image of the Pt layer of CFO/Pt@600 was found to be the [100] incident electron diffraction pattern of Pt (Figure 1g,h). This suggests that the Pt layer maintains epitaxial growth on $Co_xFe_{3-x}O_4$ (001) by deposition at 600 °C, which is consistent with the epitaxial growth of Pt on MgO.[23,24] In addition, in-plane tensile strain is also introduced in the Pt through epitaxial growth on CFO. This epitaxial strain could contribute to modulating the electronic structure of Pt.

To survey the interfacial electronic and magnetic states of Fe and Co sites, XMCD measurements at the Co and Fe *L*-edges were performed on CFO/Pt@500 and CFO/Pt@600. Figure 2a shows the XAS and XMCD spectra of CFO/Pt@500 for the Fe and Co *L*-edges. The XAS intensities of Co are suppressed owing to the composition ratio of 1:10, resulting in a composition of $Co_{0.27}Fe_{2.73}O_4$ with $x = 0.27$. The CFO with low Co composition exhibits perpendicular magnetic anisotropy (PMA).[25,26] The intensity ratio of XMCD to XAS is estimated to be 5 and 47% for the Fe and Co L_3 edges, respectively. The XAS and XMCD line shapes for Fe *L* edges show distinctive features due to three kinds of Fe states (Fe^{3+} in O_h, Fe^{3+} in T_d, and Fe^{2+} in O_h). For the Fe *L* edges, although the difference in XAS is small, clear differential XMCD line shapes are detected. The Fe^{3+} state with T_d symmetry exhibits an opposite sign, which is common for spinel-type ferrite compounds. The XMCD hysteresis curves taken at the $Fe^{3+}(O_h)$ peak photon energy are also displayed. The shapes of hysteresis curves are different between 500 and 600 °C, which is consistent with the SQUID measurements. Large XMCD signals in the Co *L* edge correspond to contribution of the orbital moment through the distorted Co^{2+} ($3d^7$) O_h site.[25,26]

The Pt growth-temperature dependence of XMCD indicates the stability of $Co_xFe_{3-x}O_4$/Pt interface structures between CFO/Pt@500 and CFO/Pt@600, except for the peak intensity ratio of Fe^{2+} (O_h) components (Figure 2b). Since XAS and XMCD spectra in the TEY probe down to a depth of less than 3 nm from the sample surface, the interfacial regions can be detected clearly. A slight increase in the $Fe^{2+}(O_h)$ component in 600 °C growth corresponds to the interfacial off-stoichiometry. The XMCD spectra of Fe were hardly dependent on the Pt film formation temperature, and the three peaks unique to the spinel oxide of Fe were maintained at CFO/Pt@600. This is a significant difference from the earlier work.[20] Consequently, there is no evidence of alloying or formation of other peculiar interface structures. From the results of HR-STEM and XMCD of Fe, the CFO/Pt interface is very well-defined and the interfacial diffusion is negligible.

Magnetic properties of the entire samples along the perpendicular magnetic fields were evaluated by SQUID. As shown in Figure 3, perpendicular magnetization was observed for both the CFO/Pt@100 and CFO/Pt@600 samples.

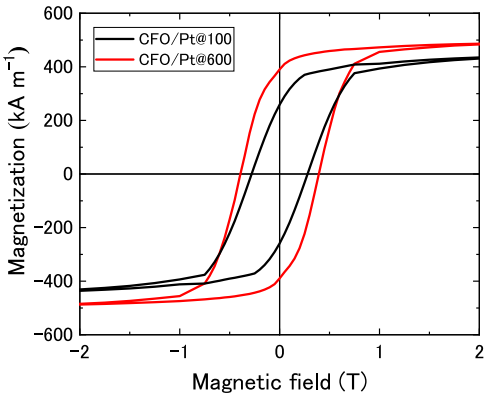

Figure 3. Magnetic hysteresis loops of CFO/Pt@100 and CFO/Pt@600 taken at RT. The magnetic field was applied perpendicular to the plane.

Therefore, the effect of Pt deposition temperature on the magnetic properties of the $Co_xFe_{3-x}O_4$ layer can be considered to be small. The difference in magnetic properties such as coercive field and remanent magnetization ratio is attributed to compositional deviation due to the codeposition of Co and Fe in CFO.[27,28]

3.2. Anomalous Hall Effect in the Pt Layer. First, we evaluated the conductivity of Pt and CFO for transport measurements. The resistivity of Pt (1 nm) and CFO (50 nm) was found to be 62×10^{-6} Ω cm and at least the order of 10^3 Ω cm, respectively. Therefore, CFO can be regarded as an insulator, and it is assumed that the current flows only in Pt in the CFO/Pt bilayers. Then, we measured the anomalous Hall effect to explore the ferromagnetism of 1 nm thick Pt. We estimated the effective Pt film thickness (t_{Pt}^{eff}) and longitudinal resistivity (ρ_{xx}^{eff}), which were used for analyzing the Hall resistivities (ρ_{AH}) from the thickness dependence of the resistance (see Section S1). Figure 4a shows the Hall conductivities ($\sigma_{AH} = -\rho_{AH}/(\rho_{xx}^{eff})2$) at RT for CFO/Pt@100 and CFO/Pt@600. An anomalous Hall effect with hysteresis was obtained for CFO/Pt for all Pt deposition temperatures. Since CFO is an insulator, the electric current flows only in the thin Pt layer, and therefore, the anomalous Hall effect could be attributed to the Pt layer. The ferromagnetic behavior of Pt in the transport properties is similar to that reported in previous studies, and the magnitudes are comparable.[12,29] The anomalous Hall effect was observed in all samples of Pt deposited at 100 °C to 600 °C. We further confirmed that this anomalous Hall effect of Pt is not spin Hall magnetoresistance (SMR) origin (see Section S2). The scaling relationship for the anomalous Hall effect was applied to estimate the mechanism of the Pt anomalous Hall effect.[30] For analysis of the scaling relationship, the anomalous Hall conductivity is defined as the value at an external magnetic field $H = 1$ T(σ_{AH}(1 T)). σ_{AH} was nearly constant, regardless of longitudinal conductivities ($\sigma_{xx}^{eff} = 1/\rho_{xx}^{eff}$), as shown in Figure 4b. In addition, the conductivity of Pt is $10^3 < \sigma_{xx} < 10^4$ Ω^{-1} cm^{-1}, which belongs to the dirty metal limit to the intermediate regime.[30] In this region, the interband transition rather than extrinsic scattering is dominant and σ_{AH} is constant and independent of σ_{xx}. This behavior is also known for $SrIrO_3$ heterostructures, and the obtained σ_{AH} is also comparable in magnitude.[31] On the other hand, this behavior is not known for the anomalous Hall effect caused by the magnetic proximity effect, suggesting that the anomalous Hall effect of CFO/Pt in this study is the intrinsic mechanism.

https://doi.org/10.1021/acsomega.3c00935
ACS Omega 2023, 8, 24875−24882

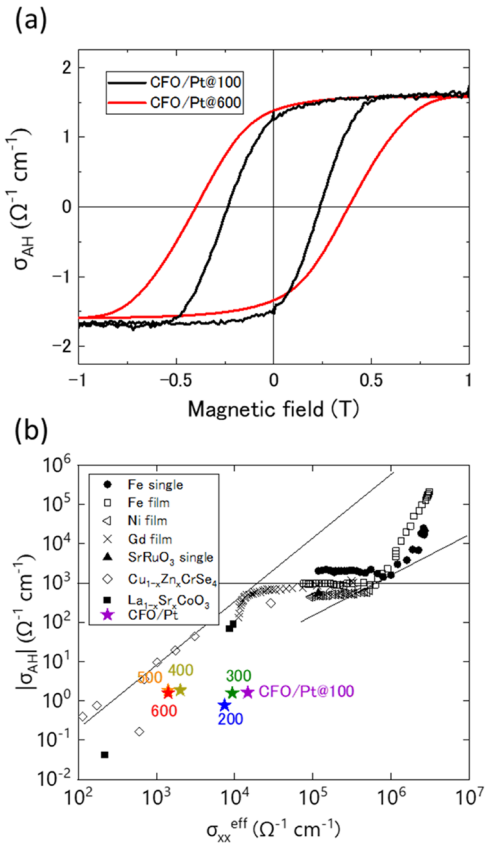

Figure 4. (a) Hall conductivity for CFO/Pt@100 and CFO/Pt@600. (b) σ_{AH} versus σ_{xx}^{eff} at H = 1 T. Both values were calculated using eq S1. See Section S1 for details. 200, 300, 400, 500, 600 in the figure correspond to CFO/Pt@200, CFO/Pt@300, CFO/Pt@400, CFO/Pt@500, CFO/Pt@600, respectively.

To explore the induced magnetism of Pt, we performed XMCD measurements at the Pt L edges. Figure 5a shows the XAS and XMCD spectra at the Pt L_3 edge of CFO/Pt@500 measured at RT. We applied a magnetic field of 1.9 T, which is sufficient to saturate the magnetization of CFO (see Figure 3). The XMCD signal was almost zero across the entire energy range, implying that the magnetic moment of Pt is negligible, at most $\mu_{Pt} < 0.001\ \mu_B$/atom, which is consistent with previous reports.[16,18,20] However, the CFO/Pt@600 sample exhibited a significant XMCD signal, although the shape of the XAS spectrum remained unchanged (Figure 5b). In contrast to the results of the Hall-effect measurements, the XMCD showed that signals originating from the ferromagnetism of Pt were obtained only for CFO/Pt@600. See Sections S2 and S3 for the analysis of the magnitude of the magnetic moment of Pt.

One reason for the significant dependence of Pt-XMCD on the deposition temperature may be the oxide ions at the interface. In the preparation process, we deposited Pt following the deposition of Fe and Co in the oxygen-radical atmosphere. Therefore, oxygen atoms existed on the surface of CFO before Pt deposition at low temperatures. The oxygen layer at the CFO/Pt interface could interfere with the electronic interaction between Pt and Co/Fe ions. For CFO@600, surface oxygen could be removed by high temperature. The absence of oxide ions at the interface allowed direct interaction between Pt and Co/Fe ions. Therefore, a clear magnetic moment of Pt originating from the MPE was observed by XMCD measurements. However, the XMCD and XAS spectra for Fe and Co were not affected by the change in deposition temperature because the spinel structure of CFO was maintained in all samples. It has been reported that the oxidation state of the interface has a considerable influence on the magnetic properties in heterostructures containing oxides.[12,32] Therefore, it is thought that the magnetic moment in Pt was induced by the direct contact between Pt and Fe or Co cations in CFO (Figure 5c,d). Another possible reason is the difference in the growth direction of Pt at different deposition temperatures. At CFO/Pt@100, Pt had a textured structure on the (111) plane, but at CFO/Pt@600, the Pt layer grew epitaxially against the CFO (001) plane. Although this could change the interaction with CFO or change the electronic structure of Pt due to the introduction of epitaxial strain (Figure 1e−h), evaluation using first-principles calculations is required to obtain a detailed understanding.

Considering the above results, we discuss the relationship between the anomalous Hall effect and induced moments of Pt in CFO/Pt via the MPE. While the anomalous Hall effect was observed in all CFO/Pt, regardless of the deposition temperature of Pt (Figure 4a,b), finite induced moments of Pt were observed in only CFO/Pt@600 (Figure 5a,b). This disagreement between the XMCD and the anomalous Hall effect measurements can be attributed to the difference in detected electrons, with the former detecting excited photoelectrons from the core levels (5d), while the latter detects conduction electrons (5s) during current flow. The anomalous Hall effect is observed, which means that the 6s electrons of Pt are spin-polarized because the Hall measurement detected the majority carriers of Pt 6s electrons.[34,35] Normally, the spin accumulation caused by the spin Hall effect in Pt[2,36] is equivalent on the left and right sides; hence, $\Delta V_{xy} \propto \rho_{AH} = 0$. ΔV_{xy} represents the electromotive force generated in the direction perpendicular to the current flow. If the 6s electrons are spin-polarized, one of the spin accumulations on the left or right side will be larger than the other, resulting in a transverse electromotive force; hence, $\Delta V_{xy} \propto \rho_{AH} \neq 0$. Therefore, it is considered that spin-polarized Pt 6s electrons produce the anomalous Hall effect. On the other hand, XMCD detects the 5d electrons of Pt, which means that the spin polarization of these 6s electrons cannot be detected.

4. CONCLUSIONS

In summary, we fabricated CFO/Pt bilayers with a well-controlled interface structure by MBE at different Pt deposition temperatures. The anomalous Hall effect was obtained, regardless of the Pt deposition temperature, which is thought to reflect the magnetic properties of the CFO layer via the MPE. However, XMCD of Pt was obtained only for the sample of Pt deposited at 600 °C, indicating that the interface structure contributes to the MPE. The HR-STEM and XMCD measurements of Co and Fe revealed no alloying at the interface. It is suggested that the slight differences in the interface structure such as an absence of oxygen ions at the interface are important for the appearance of the MPE in Pt. We believe that the results obtained in this study provide certain conclusions about the presence of MPE, which has been a topic of discussion for many years. Furthermore, the anomalous Hall effect was observed even in the sample, in which the induced moment was not obtained, suggesting that the MPE is more significant in transport properties, such as the anomalous Hall effect than in magnetic properties such as the induced magnetic moment. We expect that this result provides

https://doi.org/10.1021/acsomega.3c00935
ACS Omega 2023, 8, 24875−24882

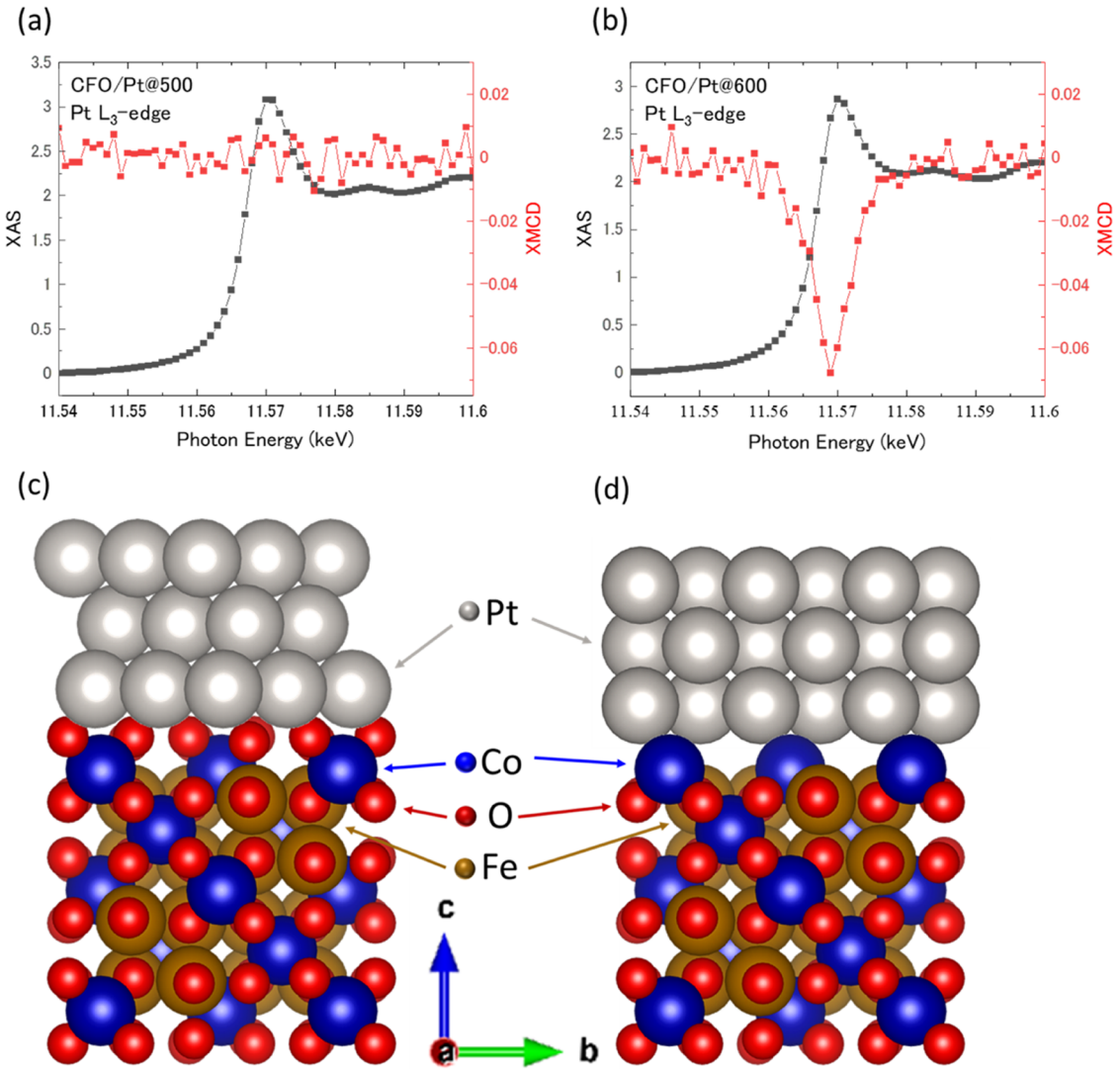

Figure 5. (a) XAS and XMCD spectra of Pt *L*-edge for CFO/Pt@500 measured at RT under an applied magnetic field of ±1.9 T. (b) XAS and XMCD spectra of Pt *L*-edge for CFO/Pt@600 measured at RT under an applied magnetic field of ± 1.9 T. Interface structure of $Co_xFe_{3-x}O_4$/Pt (c) with oxide ion and (d) without oxide ion at the interface. Panels (c, d) were rendered using VESTA software.[33]

important information for the application of FMI/HM bilayers to spintronics devices.

■ ASSOCIATED CONTENT

Supporting Information

The Supporting Information is available free of charge at https://pubs.acs.org/doi/10.1021/acsomega.3c00935.

1 nm thickness of Pt on CFO is very thin, suggesting that the effective film thickness contributing to electrical conduction (t_{Pt}^{eff}) is reduced to less than 1 nm; since the deposition temperature of Pt was significantly changed from 100 to 600 °C, t_{Pt}^{eff} among the CFO/Pt@100 to CFO/Pt@600 samples possibly varied due to the increase in surface roughness (Section S1); spin Hall magnetoresistance (SMR) effects can contribute to anomalous Hall effects in FMI/HM systems such as CFO/Pt (Section S2); measured XMCD signal of Pt is analyzed by the magneto-optic sum rule (Section S3); and thickness dependence of the magnetic moment of Pt (Section S4) (PDF)

■ AUTHOR INFORMATION

Corresponding Author

Shoto Nodo − *Graduate School of Chemical Sciences and Engineering, Hokkaido University, Sapporo 060-8628, Japan;* orcid.org/0000-0002-8656-4362; Email: punkan0511@gmail.com

Authors

Ichiro Yamane − *Graduate School of Chemical Sciences and Engineering, Hokkaido University, Sapporo 060-8628, Japan*

Motohiro Suzuki − *School of Engineering, Kwansei Gakuin University, Sanda, Hyogo 669-1330, Japan*

Jun Okabayashi − *Research Center for Spectrochemistry, The University of Tokyo, Tokyo 113-0033, Japan;* orcid.org/0000-0002-9025-2783

Seiya Yokokura − *Graduate School of Engineering, Hokkaido University, Sapporo 060-8628, Japan;* orcid.org/0000-0002-2671-8323

Toshihiro Shimada − *Graduate School of Engineering, Hokkaido University, Sapporo 060-8628, Japan;* orcid.org/0000-0001-5122-1063

https://doi.org/10.1021/acsomega.3c00935
ACS Omega 2023, 8, 24875−24882

Taro Nagahama − *Graduate School of Engineering, Hokkaido University, Sapporo 060-8628, Japan;* Present Address: Graduate School of Sciences and Technology for Innovation, Yamaguchi University, Ube, Yamaguchi, 755-8611, Japan

Complete contact information is available at: https://pubs.acs.org/10.1021/acsomega.3c00935

Notes

The authors declare no competing financial interest.

■ ACKNOWLEDGMENTS

The XMCD measurements for Pt L-edges were performed with the approval of the Japan Synchrotron Radiation Research Institute (JASRI) (Proposal No. 2020A1665). The XMCD measurements for Fe and Co L-edges were performed with the approval of the Photon Factory Program Advisory Committee, KEK (No. 2021G069). This work was partly supported by the Japan Society for the Promotion of Science (JSPS) through a research fellowship for young scientists (Grant No. 21J11984).

■ REFERENCES

(1) Dyakonov, M. I.; Perel, V. I. Current-Induced Spin Orientation of Electrons in Semiconductors. *Phys. Lett. A* **1971**, *35*, 459−460.
(2) Hirsch, J. E. Spin Hall Effect. *Phys. Rev. Lett.* **1999**, *83*, 1834−1837.
(3) Chen, Y.-T.; Takahashi, S.; Nakayama, H.; Althammer, M.; Goennenwein, S. T.; Saitoh, E.; Bauer, G. E. Theory of Spin Hall Magnetoresistance. *Phys. Rev. B* **2013**, *87*, No. 144411.
(4) Nakayama, H.; Althammer, M.; Chen, Y.-T.; Uchida, K.; Kajiwara, Y.; Kikuchi, D.; Ohtani, T.; Geprägs, S.; Opel, M.; Takahashi, S.; Gross, R.; Bauer, G. E. W.; Goennenwein, S. T. B.; Saitoh, E. Spin Hall Magnetoresistance Induced by a Nonequilibrium Proximity Effect. *Phys. Rev. Lett.* **2013**, *110*, No. 206601.
(5) Althammer, M.; Meyer, S.; Nakayama, H.; Schreier, M.; Altmannshofer, S.; Weiler, M.; Huebl, H.; Geprägs, S.; Opel, M.; Gross, R.; Meier, D.; Klewe, C.; Kuschel, T.; Schmalhorst, J.-M.; Reiss, G.; Shen, L.; Gupta, A.; Chen, Y.-T.; Bauer, G. E. W.; Saitoh, E.; Goennenwein, S. T. B. Quantitative Study of the Spin Hall Magnetoresistance in Ferromagnetic Insulator/Normal Metal Hybrids. *Phys. Rev. B* **2013**, *87*, No. 224401.
(6) Miron, I. M.; Garello, K.; Gaudin, G.; Zermatten, P.-J.; Costache, M. V.; Auffret, S.; Bandiera, S.; Rodmacq, B.; Schuhl, A.; Gambardella, P. Perpendicular Switching of a Single Ferromagnetic Layer Induced by In-Plane Current Injection. *Nature* **2011**, *476*, 189−193.
(7) Liu, L.; Pai, C.-F.; Li, Y.; Tseng, H. W.; Ralph, D. C.; Buhrman, R. A. Spin-Torque Switching with the Giant Spin Hall Effect of Tantalum. *Science* **2012**, *336*, 555−558.
(8) Fukami, S.; Anekawa, T.; Zhang, C.; Ohno, H. A Spin−Orbit Torque Switching Scheme with Collinear Magnetic Easy Axis and Current Configuration. *Nat. Nanotechnol.* **2016**, *11*, 621−625.
(9) Manna, P. K.; Yusuf, S. M. Two Interface Effects: Exchange Bias and Magnetic Proximity. *Phys. Rep.* **2014**, *535*, 61−99.
(10) Huang, S. Y.; Fan, X.; Qu, D.; Chen, Y. P.; Wang, W. G.; Wu, J.; Chen, T. Y.; Xiao, J. Q.; Chien, C. L. Transport Magnetic Proximity Effects in Platinum. *Phys. Rev. Lett.* **2012**, *109*, No. 107204.
(11) Yang, Y.; Wu, B.; Yao, K.; Shannigrahi, S.; Zong, B.; Wu, Y. Investigation of Magnetic Proximity Effect in Ta/YIG Bilayer Hall Bar Structure. *J. Appl. Phys.* **2014**, *115*, No. 17C509.
(12) Amamou, W.; Pinchuk, I. V.; Trout, A. H.; Williams, R. E.; Antolin, N.; Goad, A.; O'Hara, D. J.; Ahmed, A. S.; Windl, W.; McComb, D. W.; Kawakami, R. K. Magnetic Proximity Effect in Pt/$CoFe_2O_4$ Bilayers. *Phys. Rev. Mater.* **2018**, *2*, No. 011401(R).
(13) Ma, L.; Fu, H. R.; Tang, M.; Qiu, X. P.; Shi, Z.; You, C. Y.; Tian, N.; Zheng, J.-G. Static and Dynamic Origins of Interfacial Anomalous Hall Effect in W/YIG Heterostructures. *Appl. Phys. Lett.* **2020**, *117*, No. 122405.
(14) Liang, X.; Zhu, Y..; Peng, B.; Deng, L.; Xie, J.; Lu, M.; Wu, M.; Bi, L. Influence of Interface Structure on Magnetic Proximity Effect in Pt/$Y_3Fe_5O_{12}$ Heterostructures. *ACS Appl. Mater. Interfaces* **2016**, *8*, 8175−8183.
(15) Geprägs, S.; Meyer, S.; Altmannshofer, S.; Opel, M.; Wilhelm, F.; Rogalev, A.; Gross, R.; Goennenwein, S. T. B. Investigation of Induced Pt Magnetic Polarization in Pt/$Y_3Fe_5O_{12}$ Bilayers. *Appl. Phys. Lett.* **2012**, *101*, No. 262407.
(16) Valvidares, M.; Dix, N.; Isasa, M.; Ollefs, K.; Wilhelm, F.; Rogalev, A.; Sánchez, F.; Pellegrin, E.; Bedoya-Pinto, A.; Gargiani, P.; Hueso, L. E.; Casanova, F.; Fontcuberta, J. Absence of Magnetic Proximity Effects in Magnetoresistive Pt/$CoFe_2O_4$ Hybrid Interfaces. *Phys. Rev. B* **2016**, *93*, No. 214415.
(17) Wu, H.; Zhang, Q.; Wan, C.; Ali, S. S.; Yuan, Z.; You, J.; Wang, J.; Choi, Y.; Han, X. Spin Hall Magnetoresistance in $CoFe_2O_4$/Pt Films. *IEEE Trans. Magn.* **2015**, *51*, No. 4100104.
(18) Collet, M.; Mattana, R.; Moussy, J.-B.; Ollefs, K.; Collin, S.; Deranlot, C.; Anane, A.; Cros, V.; Petroff, F.; Wilhelm, F.; Rogalev, A. Investigating Magnetic Proximity Effects at Ferrite/Pt Interfaces. *Appl. Phys. Lett.* **2017**, *111*, No. 202401.
(19) Kuschel, T.; Klewe, C.; Schmalhorst, J.-M.; Bertram, F.; Kuschel, O.; Schemme, T.; Wollschläger, J.; Francoual, S.; Strempfer, J.; Gupta, A.; Meinert, M.; Götz, G.; Meier, D.; Reiss, G. Static Magnetic Proximity Effect in Pt/$NiFe_2O_4$ and Pt/Fe Bilayers Investigated by X-Ray Resonant Magnetic Reflectivity. *Phys. Rev. Lett.* **2014**, *115*, No. 097401.
(20) Vasili, H. B.; Gamino, M.; Gàzquez, J.; Sánchez, F.; Valvidares, M.; Gargiani, P.; Pellegrin, E.; Fontcuberta, J. Magnetoresistance in Hybrid Pt/$CoFe_2O_4$ Bilayers Controlled by Competing Spin Accumulation and Interfacial Chemical Reconstruction. *ACS Appl. Mater. Interfaces* **2018**, *10*, 12031−12041.
(21) Seto, Y.; Ohtsuka, M. ReciPro: Free and Open-source Multipurpose Crystallographic Software Integrating a Crystal Model Database and Viewer, Diffraction and Microscopy Simulators, and Diffraction Data Analysis Tools. *J. Appl. Crystallogr.* **2022**, *55*, 397−410.
(22) Nodo, S.; Ono, S.; Yanase, T.; Shimada, T.; Nagahama, T. Controlling the Magnetic Proximity Effect and Anomalous Hall Effect in $CoFe_2O_4$/Pt by Ionic Gating. *Appl. Phys. Express* **2020**, *13*, No. 063004.
(23) McIntyre, P. C.; Maggiore, C. J.; Nastasi, M. Orientation Selection in Thin Platinum Films on (001) MgO. *J. Appl. Phys.* **1995**, *77*, 6201−6204.
(24) Ahn, K. H.; Baik, S.; Kim, S. Change of Growth Orientation in Pt Films Epitaxially Grown on MgO (001) Substrates by Sputtering. *J. Mater. Res.* **2002**, *17*, 2334−2338.
(25) Okabayashi, J.; Tanaka, M. A.; Morishita, M.; Yanagihara, H.; Mibu, K. Origin of Perpendicular Magnetic Anisotropy in $Co_xFe_{3-x}O_{4+\delta}$ Thin Films Studied by X-Ray Magnetic Circular and Linear Dichroisms. *Phys. Rev. B* **2022**, *105*, No. 134416.
(26) Morishita, M.; Ichikawa, T.; Tanaka, M. A.; Furuta, M.; Mashimo, D.; Honda, S.; Okabayashi, J.; Mibu, K. Control of conductivity in Fe-rich cobalt-ferrite thin films with perpendicular magnetic anisotropy. *Phys. Rev. Mater.* **2023**, *7*, No. 054402.
(27) Yanagihara, H.; Utsumi, Y.; Niizeki, T.; Inoue, J.; Kita, E. Perpendicular Magnetic Anisotropy in Epitaxially Strained Cobalt-Ferrite (001) Thin Films. *J. Appl. Phys.* **2014**, *115*, No. 17A719.
(28) Moyer, J. A.; Vaz, C. A. F.; Kumah, D. P.; Arena, D. A.; Henrich, V. E. Enhanced Magnetic Moment in Ultrathin Fe-Doped $CoFe_2O_4$ Films. *Phys. Rev. B* **2012**, *86*, No. 174404.
(29) Tang, C.; Sellappan, P.; Liu, Y.; Xu, Y.; Garay, J. E.; Shi, J. Anomalous Hall Hysteresis in $Tm_3Fe_5O_{12}$/Pt with Strain-Induced Perpendicular Magnetic Anisotropy. *Phys. Rev. B* **2016**, *94*, No. 140403.
(30) Miyasato, T.; Abe, N.; Fujii, T.; Asamitsu, A.; Onoda, S.; Onose, Y.; Nagaosa, N.; Tokura, Y. Crossover Behavior of the

Anomalous Hall Effect and Anomalous Nernst Effect in Itinerant Ferromagnets. *Phys. Rev. Lett.* **2006**, *99*, No. 086602.
(31) Jaiswal, A. K.; Wang, D.; Wollersen, V.; Schneider, R.; Tacon, M. L.; Fuchs, D. Direct Observation of Strong Anomalous Hall Effect and Proximity induced Ferromagnetic State in $SrIrO_3$. *Adv. Mater.* **2022**, *34*, No. 2109163.
(32) Zhang, X.-G.; Butler, W. H.; Bandyopadhyay, A. Effects of the Iron-Oxide Layer in Fe-FeO-MgO-Fe Tunneling Junctions. *Phys. Rev. B* **2003**, *68*, No. 092402.
(33) Momma, K.; Izumi, F. VESTA 3 for Three-Dimensional Visualization of Crystal, Volumetric and Morphology Data. *J. Appl. Crystallogr.* **2011**, *44*, 1272−1276.
(34) Windmiller, L. R.; Ketterson, J. B.; Hornfeldt, S. Experimental Determination of the Fermi Radius, Velocity, and g Factor in Pd and Pt. *J. Appl. Phys.* **1969**, *40*, 1291−1293.
(35) Andersen, O. K. Electronic Structure of the Fcc Transition Metals Ir, Rh, Pt, and Pd. *Phys. Rev. B* **1970**, *2*, 883−906.
(36) Kimura, T.; Otani, Y.; Sato, T.; Takahashi, S.; Maekawa, S. Room-Temperature Reversible Spin Hall Effect. *Phys. Rev. Lett.* **2007**, *98*, No. 156601.

https://doi.org/10.1021/acsomega.3c00935
ACS Omega 2023, 8, 24875−24882